Geomechanics and Engineering, *Vol. 39, No. 2 (2024) 197-209*
https://doi.org/10.12989/gae.2024.39.2.197

Deformation of large-diameter pipeline induced by double shield tunneling in silty fine sand strata

Ning Jiao[1a], Jianwen Ding*[1], Zhaosheng Liao[2b], Xing Wan[1c] and Xia Wei[1d]

[1]*Institute of Geotechnical Engineering, School of Transportation, Southeast University, No.2, Southeast Road, Jiangning District, Nanjing, 211189, China*
[2]*Direct Affairs Center of the Yiyang Transportation Bureau, Yiyang, 413000, China*

(*Received July 18, 2021, Revised September 30, 2024, Accepted October 10, 2024*)

Abstract. This paper investigated the deformation of a large-diameter pipeline caused by double shield tunnel construction in silty fine sand strata in Nantong, China, by on-site measurements and numerical simulations. Results indicate the pipe settlement curve was not symmetrical after the double tunnel construction in the silty fine sand strata. The construction of the subsequent tunnel had a significantly smaller impact on the stress and horizontal displacement of the pipeline than the preceding tunnel. There is a significant shading effect of the large-diameter pipeline, which would restrict the soil settlement above the pipeline. The adjusted settlement formula shows good agreement with the measured data, facilitating approximate calculations for both surface and pipe settlements. The correction factor a ranges from 0.50 to 0.90, while b ranges from 0.95 to 1.20.The elastic modulus and the burial depth of the pipeline had a great effect on the stress of the pipeline, but a smaller effect on its settlement. However, the soil loss rate greatly affected both the settlement and stress of the pipeline. Moreover, the pipeline risk level distribution map can quickly identify the risk status of the pipeline.

Keywords: double shield tunneling; field tests; large-diameter pipeline; numerical simulation; pipeline deformation; silty fine sand strata

1. Introduction

With the development of urbanization, rail transit was considered an efficient method to resolve traffic congestion with its convenient and great delivery capabilities (Mackett *et al.* 1998, Katebi *et al*. 2015). Shield method was extensively adopted in tunnel construction due to its high security, rapid digging speed and high automatization (Rowe *et al*. 1983, Asakura and Kojima 2003, Jeon *et al*. 2020). Notably, it is inevitable that most urban shield tunnels cross areas with densely distributed underground municipal pipelines. Additional loads will be generated by the pipe-soil interaction during construction, leading to the deformation of the adjacent pipeline, which may threaten the normal use of the pipeline. Especially for large-diameter pressure pipelines, excessive deformation could lead to leakage or even fracture of the pipeline and other accidents (Vorster *et al*. 2005, Klar and Marshall 2016, Heama *et al*. 2021).

Impacts of shield tunneling for adjacent pipes have been investigated by many scholars through field measurement, numerical simulation, theoretical analysis, and model test (Klar *et al*. 2007, Civalek *et al*. 2010, Wham *et al*. 2016, Boulefrakh *et al*. 2019, Huang *et al*. 2019, Zhu *et al*. 2020, Sae-Long *et al*. 2021, Joshi *et al*. 2024). It was investigated the relative position of pipes and tunnels, as well as the construction method of the double tunnel, have a great impact on pipeline deformation. Pipeline diameter, pipeline buried depth, and excavation method played a dominant role in pipeline stress (Klar *et al*. 2008, Liu *et al*. 2012, Deng *et al*. 2021). In addition, soil properties, especially soil loss rates, were also the dominant factors of the stress and deformation in the pipeline (Marshall *et al*. 2010,Zhang *et al*. 2012). Moreover, it was found that grouting reinforcement could effectively reduce the settlement of the pipeline, and the pipeline deformation was minimized as the deep-hole grouting reinforcement range was larger than 0.3 times the distance between the pipeline and tunnel (Wang *et al*. 2021).

Based on an actual project of a shallow buried tunnel crossed the large-diameter buried pipeline, Li *et al*. (2020) studied the settling law for pipes and ground surface under the tunnel-soil-pipe interaction through field measurements. The results indicated that monitoring ground subsidence over large-diameter pipelines can effectively replace direct pipeline monitoring (Joshi *et al.* 2023b), and that ground settlement could be used as an empirical guideline for judging the security of the pipeline. Sun *et al*. (2021) investigated the responded of existed pipelines due to non-

*Corresponding author, Professor
E-mail: jwding@seu.edu.cn
[a]Ph.D. Student
E-mail: jiaoning@seu.edu.cn
[b]Junior Engineer,
E-mail: 646393946@qq.com
[c]Ph.D. Student
E-mail: wanxing1994@seu.edu.cn
[d]Graduate Student
E-mail: 220213354@seu.edu.cn

ISSN: 2005-307X (Print), 2092-6219 (Online)

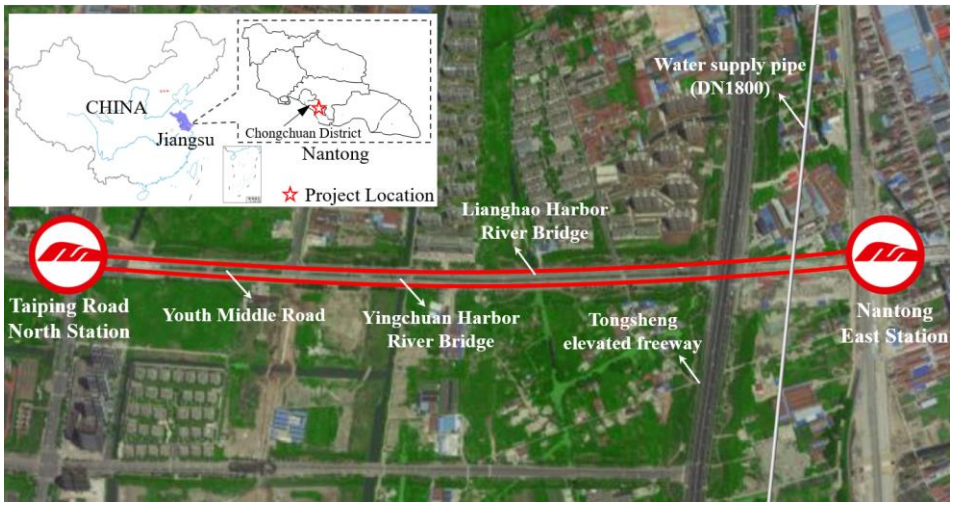

Fig. 1 Project location

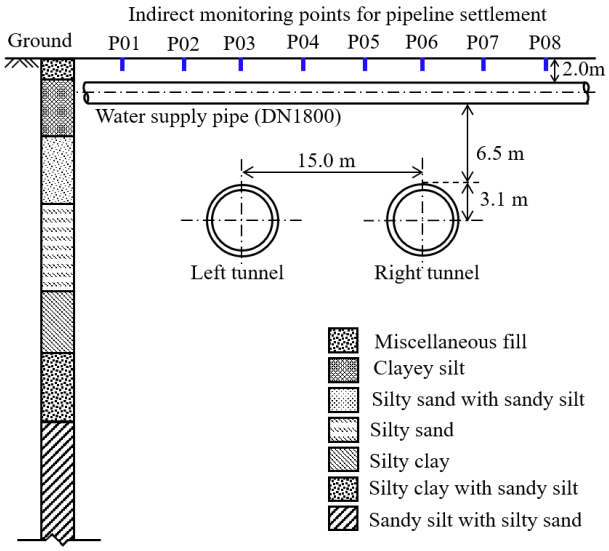

Fig. 2 Cross-section of shield construction crossing pipe

synchronous boring of double tunnels in clay strata by numerical simulation. Results indicated that the settlement curve of the pipeline transferred from V-shape to W-shape with the decreasing pipeline-soil relative stiffness. The pipe settling curve maintained basically symmetry, with the maximum settlement of the pipeline occurring above the central axis of the twin tunnels. Results indicated that the settlement curve of the pipeline transferred from V-shape to W-shape with the decreasing pipeline-soil relative stiffness. The pipe settling curve maintained basically symmetry, with the maximum settlement of the pipeline occurring above the central axis of the twin tunnels.

Although some research has been conducted, the silty fine sand surrounding the pipeline remains highly susceptible to disturbance from shield construction due to its loose texture, permeability, and low bearing capacity. This vulnerability can result in leaks or fractures, particularly in large-diameter pressure pipelines. (Liu *et al*. 2019, Zhang *et al*. 2021). At present, the effect regularity is still unclear about the double shield tunneling on the pipelines in silty fine sand strata. Thus, a case study of the pipeline deformation was presented based on a double shield tunnel in Taiping Road North-Nantong East Station Metro line 2, in the silty fine sand strata in Nantong, China. The effects of pipeline diameter, pipeline buried depth, and soil characteristics on pipeline deformation were analyzed by field measurement and numerical simulation.

2. Project overview

The shield zone between Taiping Road North Station and Nantong East Station of Nantong Metro Line 2 was located in the Chongchuan District of Nanton, China. As shown in Fig. 1, the shield tunnels were laid eastward along Youth Middle Road after started from Taiping Road North Station, crossed two river bridges and an elevated bridge in sequence, and finally crossed a large-diameter water supply

pipe before entered the Nantong East Station. The shield zone consisted of two tunnels with a total length of 1.879 km, separated by 13 to 17 m. The tunnel burial depth ranged from 9.3 m to 17.9 m, with an external diameter of 6.2 m. The width, thickness, and concrete grade of the shield lining segments were 1200 mm, 350 mm, and C50, respectively. The right tunnel was bored after the completion of the left tunnel.

The water supply pipe traversed by tunnels was a spheroidal cast iron pipe with 1.8 m diameter and 28 mm wall thickness in medium pressure. Its burial depth was about 2.0 m, and the distance from the top of the tunnel was 6.5 m, as shown in Fig. 2. Eight direct monitoring points at 5 m intervals above the tunnel were installed to monitor the pipe settlement during the construction.

Besides, Ground surface settlement monitoring points were installed along the tunnel axis, with standard sections set every 35 meters. For the first 60 m, monitoring sections were placed every 5 m; from 60 to 120 m, they were spaced every 15 m; and beyond 120 m, every 35 m. Each section included 11 points, spaced approximately every 3 m along the tunnel axis and at 3, 5, and 10 m intervals outside the axis.

3. Field measurement results and discussion

3.1 Analysis of monitoring data

The pipeline settlement at different construction stages during the left tunnel construction was presented in Fig. 3(a). The pipeline occurred uplift before the excavation face reached below the pipeline, with the maximum uplift value of 2 mm occurring above the tunnel axis. This should be mainly attributed to the larger shield thrust, increased friction of the shield body on the surrounding soil, and increased pressure in the soil chamber (Liu *et al*. 2012, Rezaei *et al*. 2019). A certain degree of fluctuation was observed in the pipeline settlement during the tunnel boring, after which the vertical displacements of the pipeline above the tunnel axis gradually changed from uplift to settlement. As the excavation face passed 6 m through the pipeline, the shield tail reached below the pipeline and a large settlement occurred in the pipeline, with a maximum value of 3.2 mm occurring above the tunnel axis. This was mainly attributed to the untimely grouting at the shield tail and the soil loss by voids, resulting in a large settlement of the soil. After the excavation face passed the pipeline 9 m, a certain degree of uplift was observed in the whole pipeline with the grouting behind segments. Thereafter, the pipeline settlement increased as the soil consolidated, and the final settling curve conformed to the Gaussian distribution, with a final settlement of about 3 mm.

The settlements of typical monitored points with the left tunnel construction were shown in Fig. 3(b). A certain degree of uplift occurred was observed in the pipeline before the excavation face reached, and the value of the uplift at P04 was greater than that at P03. The vertical displacement of P03 gradually changed to settlement as the excavation face crossed the pipeline, whereas that of P04

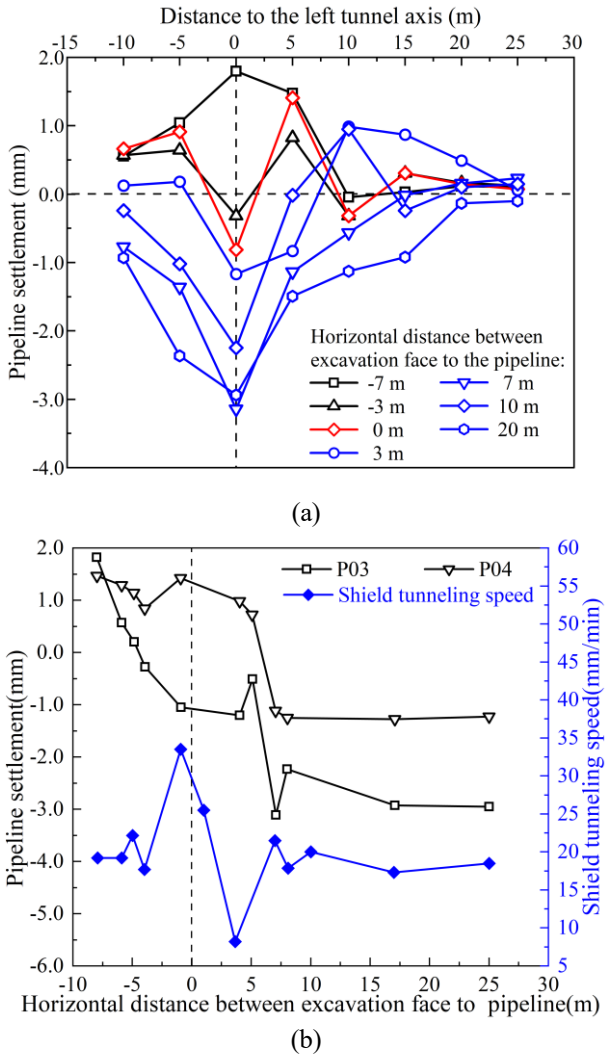

Fig. 1 Pipeline settlement during left tunnel construction: (a) Settlement at different construction stages and (b) Settlement of typical monitoring points

remained uplifted. This should be attributed to the different deformations of the surrounded soil resulting from the friction of the shield body and the rotation of the shield cutterhead. It may also be explained by the relatively larger tunneling speed of 33 mm/min at this point. The pipeline settlement increased rapidly as the shield tail crossed the pipeline, and the incremental settlement of P03 and P04 at this stage accounted for 60.2% and 54.2% of the total settlement increment, respectively. This indicates the strata loss caused by the voids of the shield tail was mainly responsible for the pipeline settlement.

To guarantee the safety and stability of the pipeline, the shield tunneling speed was constantly maintained at a low level in the process of crossing the pipeline, which was only 44.4% to 73.0% of the normal tunneling speed in this project (45 mm/min). After the left tunnel construction, the largest settlement of the pipeline was about 3 mm, which was much smaller than the settlement limit of the rigid pressurized pipeline. This indicates that keeping a low speed of shield tunneling through pipelines could efficiently reduce the impact of shield construction on pipelines, which

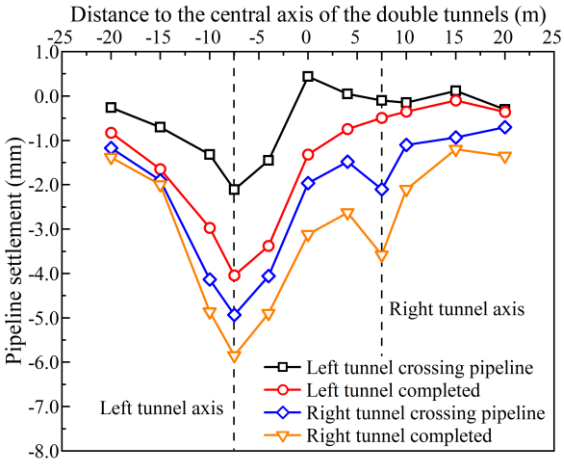

Fig. 2 Ground surface settlement at 10 m from the pipeline

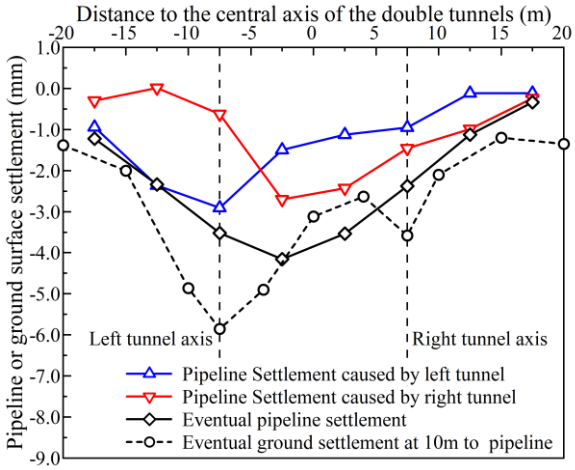

Fig. 3 Pipeline settlement for double shield construction

is similar to the conclusion that shield tunneling speed has significant effects on the stability of the strata by Hu *et al*. (2021).

3.2 Impact of double tunnel construction

Fig. 4 illustrated the settlements of ground surface at 10 m from the pipeline. The phrase "10 m from the pipeline" refers to a lateral distance measured horizontally from the pipeline. The surface settlement over the tunnel gradually increased with the left tunnel construction until its completion, and the settling curve was featured with V-shape, with the maximum settlement occurring over the left tunnel axis. With the right tunnel boring, a significant surface settlement occurred above the left tunnel, except that above the right tunnel. The final settlement curve was featured with W-shaped, and the increase above the left tunnel axis accounted for 37.5% of the final settlement during this phase. This indicates that there was a remarkable settlement superposition effect and a secondary disturbance effect for the double tunnel construction.

Compared with other typical engineering data, the secondary disturbance effect caused by the subsequent shield tunneling in the silty fine sand strata was found to be greater than that in the clay and silty strata, but less than that in the sand strata. This was attributed to the lower cohesion and the looseness structure of the sand and silty fine sand, which were more susceptible to construction disturbance (Chen *et al*. 2011, Mathew and Lehane 2013, Ocak 2013).

The pipeline settlement for the double tunnel construction was shown in Fig. 5. The pipeline settlements induced by the right tunnel boring was still consistent with the normal distribution. However, the settling curve was not completely symmetrical, with the pipeline settlement larger in the upper part of the left tunnel than in the right tunnel. This is clearly different from the conclusion drawn by Sun *et al*. (2021), which showed a perfectly symmetrical pipeline settlement curve after the double tunnel construction in clay strata.

Besides, the pipeline settlement, which was also the surface settlement over the pipeline, was remarkably less than the ground settlement 10 m away, this may be explained by the shading effect of the pipeline (Shi 2015).

The shading effect of the pipeline refers to its influence on the surrounding soil settlement. Due to the rigid nature of the pipeline, it can alter the pressure distribution, resulting in a reduction in the settlement rate of the surrounding soil and causing stress concentration, which in turn affects the deformation and safety of the pipeline. Furthermore, the presence of the pipeline can change the deformation pattern of the soil, particularly under different soil layer conditions, where this effect is even more pronounced. Different from the W-shape curve of the ground settlement, the final pipeline settling curve was featured with V-shape. It was mainly attributed to the continuity and integrity of the pipeline deformation, which was similar to the characteristics of continuous beams and could transfer the bending moment itself.

3.3 Modification of the formula coefficients

Shield excavation induces ground and pipeline settlement primarily due to surface loss, stress redistribution, soil deformation, and subsequent soil reconsolidation (Marshall *et al*. 2010). Factors such as working face thrust, grouting pressure, cutter torque, and shield machine vibration further affect the surrounding soil during excavation. Therefore, accurately estimating ground and pipeline settlement is a complex task. Peck (1969) proposed empirical formulas (Eqs. (1) and (2)) based on extensive tunneling project data for calculating ground settlement.

$$S = S_{\max} \exp\left[-\frac{x^2}{2i^2}\right] \tag{1}$$

$$S_{\max} = \frac{V_{loss}}{i\sqrt{2\pi}} = \frac{\pi R^2 \eta}{i\sqrt{2\pi}} \tag{2}$$

Where $S_{\max}$ denotes the maximum ground surface settlement (S), i denotes the width of the ground surface settlement trough, η denotes the rate of formation loss (V_{loss}).

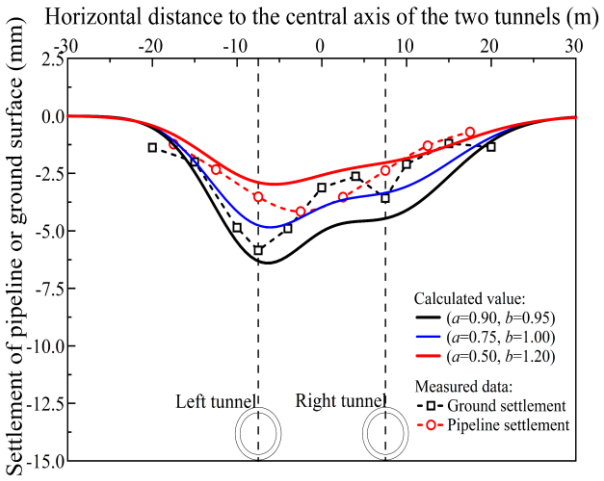

Fig. 4 Comparison between measured data and calculated values by the modified equation

Ding *et al*. (2021) modified the settlement formula by introducing a surface settlement correction factor (a) and a sinkhole width correction factor (b) in Eq. (3).

$$S = aS_{\max} \exp\left[-\frac{x^2}{2(bi)^2}\right] \tag{3}$$

In the context of double shield tunnels, the settlement profile is complex and not simply the sum of left and right tunnel effects due to their interactions. Suwansawat and Einstein (2007) developed an improved equation using the hypergeometric method to predict surface settlement for double shield tunnels, presented in Eq. (4).

$$S(x) = S_{\max 1} \exp\left[-\frac{(x-0.5L)^2}{2i_1^2}\right] + S_{\max 2} \exp\left[-\frac{(x+0.5L)^2}{2i_2^2}\right] \tag{4}$$

$$S(x) = \frac{a\pi R^2 \eta_1}{bi_1\sqrt{2\pi}} \exp\left[-\frac{(x-0.5L)^2}{2(bi_1)^2}\right] + \frac{a\pi R^2 \eta_2}{bi_2\sqrt{2\pi}} \exp\left[-\frac{(x+0.5L)^2}{2(bi_2)^2}\right] \tag{5}$$

Jiao *et al*. (2024) observed that the settlement of the leading tunnel face in a double shield tunnel is influenced by the construction of the trailing face and does not follow a straightforward superposition. Thus, Eq. (4) was revised and expanded to derive Eq. (5).

Since the settlement equation considers soil loss rates and sinkhole widths, it remains valid regardless of whether pipes are present in the soil (Sun *et al*. 2021). Large diameter pipelines typically use robust materials, enhancing their rigidity and load-bearing capacity, thereby moderating the impact of soil settlement on them. Consequently, pipeline settlement closely approximates ground settlement. Therefore, by adjusting the correction coefficient appropriately, modified formula (5) can effectively calculate both ground and pipeline settlements.

To ascertain the appropriate range for the correction coefficients, typical surface and pipeline settlement measurements were compared against the calculated values from the adjusted equation, as depicted in Fig. 6. It is evident that the corrected settlement equation aligns well with the observed data. By reverse calculation, the upper and lower bounds of the correction coefficients for the settlement equations were determined. Specifically, correction factor (a) ranges from 0.50 to 0.90, while (b) ranges from 0.95 to 1.20.

4. Numerical simulation analysis

4.1 Model establishment

A 3D model was established with Plaxis 3D on the basis of the project profile, as shown in Fig. 7(a). It should be noted that the angle of intersection between the twin tunnels and the piled foundations is not precisely 90 degrees. For modeling purposes, this intersection angle was simplified to 90 degrees in the 3D model. The soil layer was simulated using the Hardening model of Small Strain (HSS), since the HSS model integrates the shear hardening and compression hardening of the soil, which is more applicable to the soft strata such as the silty fine sand and clay. (Jal-low *et al*. 2019). The physical and mechanical parameters of the soils were adopted from the geological survey report of the site in addition to references to relevant codes and standards. The process involves field sampling followed by laboratory tests focusing on assessing physical properties, compressive strength, shear strength and deformation modulus, as shown in Table 1. The model was free-form at the top, with double-edge restrainted at the bottom. (Möller and Vermeer 2008, Nawel and Salah 2015).

The construction of 54 ring segments, each 1.2 meters wide, was simulated for both the left and right tunnels, with the exception of the initial stage, which was established as an already constructed 15 m. To enhance accuracy in the simulation, only one excavation and support ring segment was modeled for each phase. The water supply pipe was perpendicular to the tunnel, 1.8 m in diameter and 80 m long, and located at half the width of the model. The tunnel segment was simulated with solid units, and the shield machine and water supply pipeline are simulated with plate units, without considering the water pressure inside the pipe. Their property factors are presented in Table 2. Interface units were set up to simulate slab-soil interactions between the tunnel and the surrounding soil and between the pipe and the surrounding soil. The FEM mesh was created at medium density in the whole model and at fine density in the pipe and tunnels as well as the soil around them, as shown in Fig. 7(b). The model consists of 139,987 ten-node tetrahedra with 227,623 nodes after the completion of the meshing (Hasanpour 2014, Li *et al*. 2020, Sarfarazi and Tabaroei 2020, *Joshi et al*. 2023a).

Morever, the equilibrium pressure at the excavation face was calculated according to the equation as follows. Where γ_i and h_i represent the weight and the thickness of layer i soil, φ denotes the internal friction angle

$$P_0 = \sum_{i=1}^{n} (1-\sin\varphi')\gamma_i h_i \tag{6}$$

Based on field construction parameters, the jack thrust was measured at 800 kPa, while the grouting pressure at the shield tail was approximately 1.1 to 1.2 times the

Table 1 Physico-mechanical parameters of the stratum

Soil Materials	Thickness (m)	Gravity (kN/m^3)	Effective cohesion (kPa)	Effective internal friction angle (°)	Elastic modulus (MPa)			
					E_{50}^{ref}	E_{oed}^{ref}	E_{ur}^{ref}	G_0^{ref}
Miscellaneous fill	1.8	18.5	18.0	12.0	6.12	5.10	18.30	14.65
Clayey silt	4.9	18.3	17.1	20.0	4.23	3.84	12.70	10.10
Silty sand with sandy silt	5.6	19.3	6.6	31.5	8.45	7.69	25.40	20.30
Silty sand	7.2	19.1	5.0	32.4	7.76	7.06	23.30	18.60
Silty clay	5.3	17.5	22.5	15.3	2.62	2.38	7.85	6.28
Silty clay with sandy silt	5.7	17.9	18.2	18.7	3.56	3.23	10.70	8.53
Sandy silt with silty sand	-	18.0	13.5	27.9	5.34	4.85	16.00	12.80

Note：E_{50}^{ref}—Secant modulus; E_{oed}^{ref}—Tangent modulus; E_{ur}^{ref}—Unloading/reloading modulus; G_{f0}^{re}—Shear modulus

Table 2 Mechanics parameters of structural members

Structural members	Thickness (mm)	Gravity (kN/m^3)	Elastic modulus (GPa)	Shear modulus (GPa)	Poisson's ratio
Shield tunneling machine	350	120.0	23.0	11.5	0
Shield segment	350	27.0	31.0	15.5	0.1
Water supply pipe	28	72.5	155.0	77.5	0.25

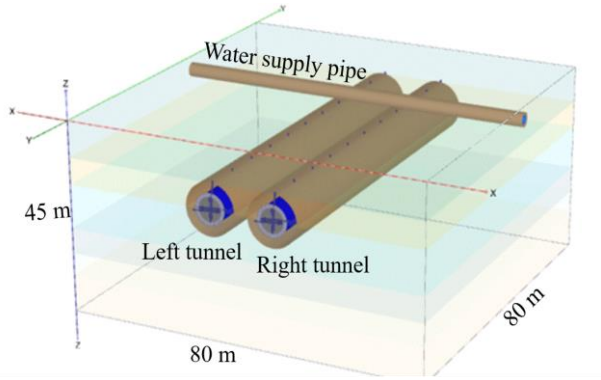

(a)

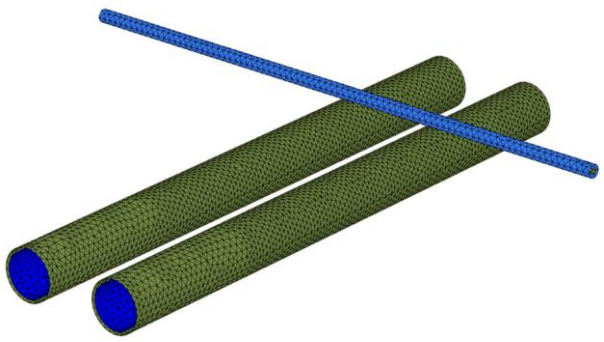

(b)

Fig. 5 The 3D FEM model: (a) Distribution of the pipe and tunnels and (b) Meshing of the pipe and tunnels

equilibrium pressure at the excavation face. Using the stratigraphic parameters from Table 1, the equilibrium pressure at the excavation surface was calculated to be 107.7 kPa, increasing with depth at a rate of 9.2 kPa/m. The grouting pressure was set at 120.0 kPa, rising with depth at a rate of 11.0 kPa/m. Additionally, the overcutting effect was simulated by applying soil loss coefficients.

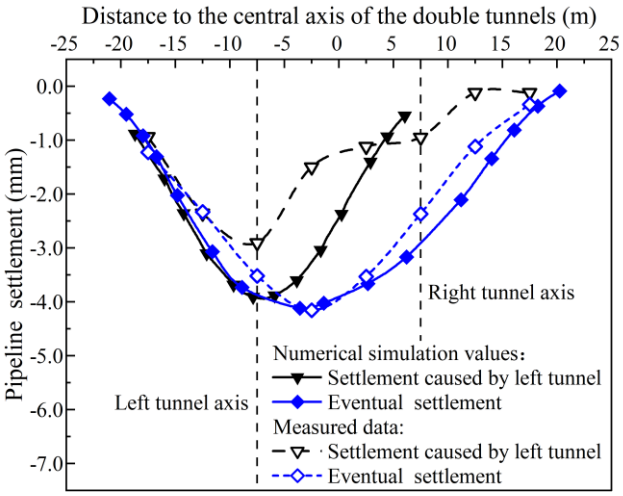

Fig. 6 Comparison between numerical simulation values and measured data

4.2 Validation by field data

The comparison of the calculated pipeline settlement through numerical simulation and measurement was presented in Fig. 8. The pipeline settling curves of the simulated agreed with monitoring results well, and also conformed to the Gaussian distribution. At the end of left tunnel boring, the greatest settlement of numerical simulation results was larger than that of the measured data, with a difference of 0.9 mm. However, the maximum pipeline settlement obtained from the numerical simulation after the construction of the double tunnels was almost equal to that of the measured data. In general, the established numeration model could simulate the pipeline deformation effectively and precisely.

Table 3 Physical and mechanical parameters for different material pipelines

Pipeline Material	Density (kN/m^3)	Elastic modulus (GPa)	Poisson's ratio
PE	17.5	9.0	0.27
Concrete	24.0	34.5	0.20
Cast iron	72.5	155.0	0.25

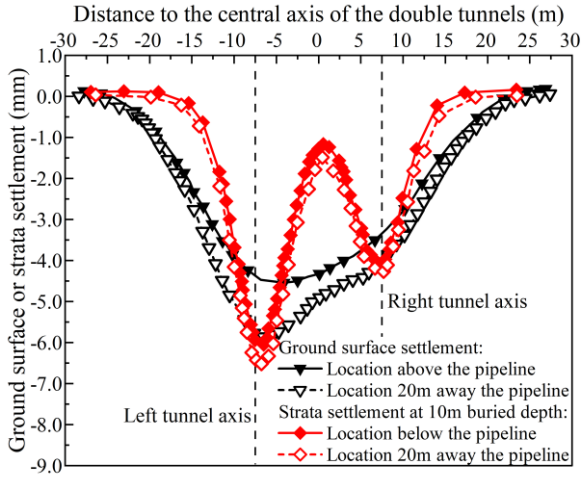

Fig. 7 Settlements of ground and stratum surrounding the pipeline

4.3 Numerical simulation results and discussion

4.3.1 Stratigraphic settlement

Fig. 9 presented the settlement of ground and stratum surrounding the pipeline. The ground surface settling curve above the pipeline was V-shape with a maximum settlement of 4.5 mm, whereas that 20 m away was featured W-shaped with a maximum settlement of 5.8 mm. The strata settlement curves below the pipeline location (10 m burial depth) and that 20 meters away at the same depth all were featured with W-shaped, with almost no difference in settlement values and settlement trough width between them. It was indicated that the settlement of soil was restricted with the shading effect produced by the existence of the pipeline, and the restricting effect on the soil above the pipeline was obviously greater than that below the pipeline. This mainly resulted from that the pipeline was similar to a continuous beam structure fixed at both ends, it had a certain bearing capacity that enabled to restrict the soil settlement above the pipeline. It also verified the speculation in the analysis of the measured data.

4.3.2 Pipeline horizontal displacement

The pipeline lateral displacement after the double tunnels construction was presented in Fig. 10. Positive horizontal displacement refers to movement in the direction of the tunnel boring machine, while negative horizontal displacement indicates movement away from the tunnel boring machine. An obviously opposite horizontal displacement was observed in the top and bottom of the

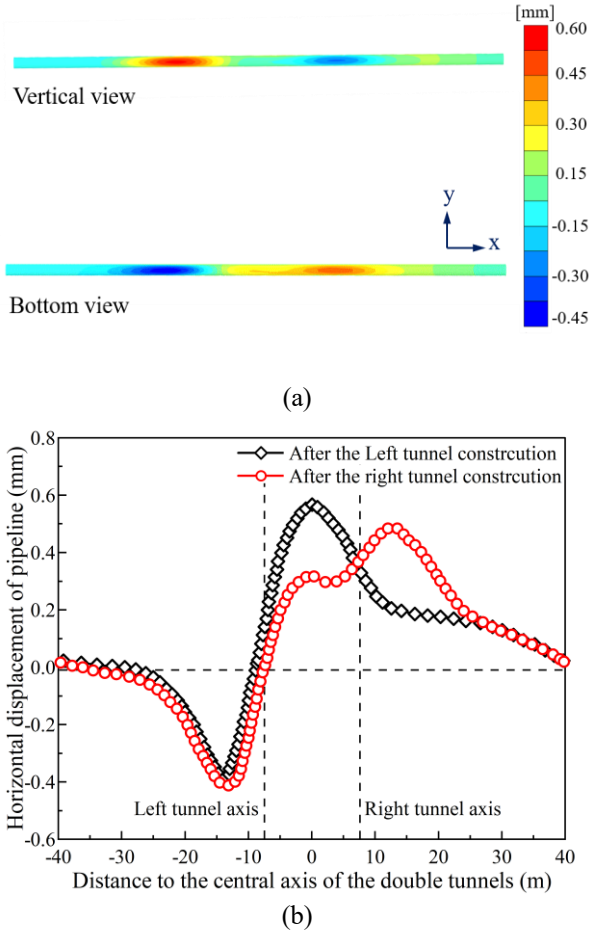

Fig. 8 Horizontal displacement of the pipeline after the construction: (a) Horizontal displacement nephogram after double tunnel construction and (b) Horizontal displacement of the lower part of the pipeline

pipeline. After the construction of the left tunnel, the lower part of the pipeline on each side above the left tunnel axis produced horizontal displacement in the direction away from the tunnel axis, respectively. The horizontal displacements of the pipeline at the left side of the left tunnel axis were nearly unchanged after the right tunnel construction, but that on the right side decreased by a certain degree. This was attributed to the reduction in the horizontal frictional resistance between the pipeline and soil caused by the disturbance of the surrounding soil in the right tunnel excavation.

4.3.3 Stress of the pipeline

The pipeline stresses for various shield constructing stages were presented in Fig. 11. Pipeline stress specifically referred to the normal stresses experienced by the pipeline during various stages of shield construction. The stresses in the upper and lower parts of the pipeline at the same cross-section were opposite during the construction, with the top part mostly affected by compressive stress and the bottom part mostly affected by tensile stresses. The compressive and tensile stresses reached the maximum of 12.0 MPa and

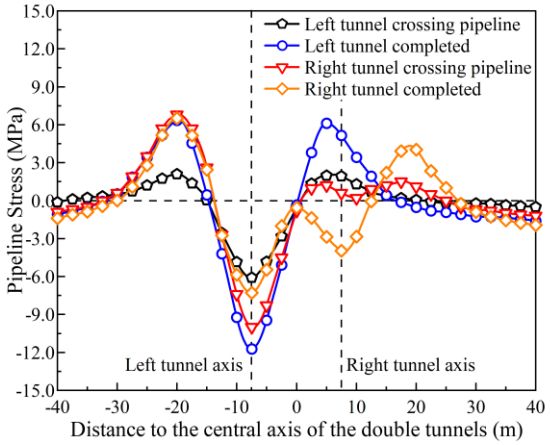

(a)

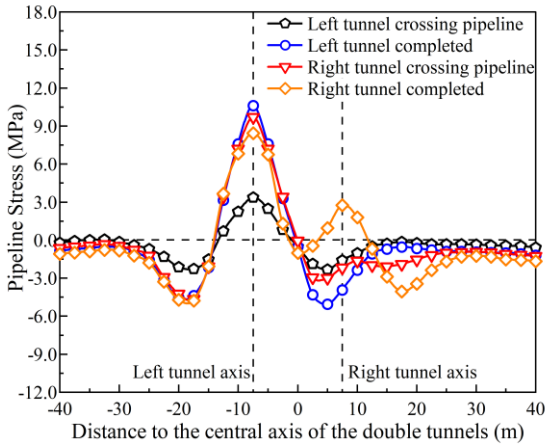

(b)

Fig. 9 Normal stresses in pipelines at different construction stages: (a) Top part of the pipeline and (b) Bottom part of the pipeline

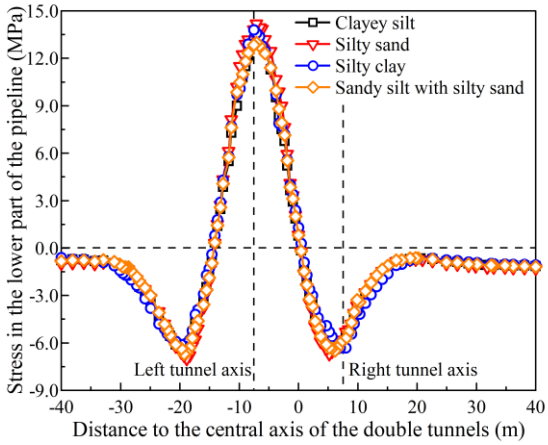

(a)

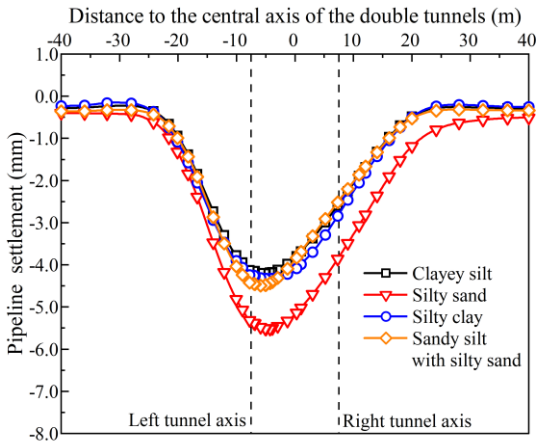

(b)

Fig. 10 Settlement and stress of pipes in different soil formations: (a) Stress after the left tunnel construction and (b) Pipeline settlement after double tunnel construction

11.0 MPa, respectively, as the left tunnel construction was completed, both occurred above the left tunnel axis. The pipeline stress gradually decreased during the right tunnel construction, and the stress in the upper part of the pipeline, within 1.2 times the tunnel diameter on both sides of the right tunnel axis, gradually changed from tensile to compressive, but that in the lower part changed from compressive to tensile. In general, the effect of subsequent tunnel construction on pipeline stress was much less than that of the preceding tunnel, which was consistent with the finding of Guan *et al*. (2020).

The pipeline material in this project was ink ductile iron, its maximum allowable compressive and tensile stresses were over 150 Mpa. Therefore, the pipeline was considered to be in a safe and stable condition with maximum stress within the allowable limits. However, the tensile strength of large-diameter pipelines made of concrete and cast iron was much less than the compressive strength, resulting in vulnerability to tensile damage.

4.4 Parametric analysis

4.4.1 Soil properties

During the construction of the tunnel, there is a difference in the deformation of the pipeline in the different strata, which is attributed to the closely related pipeline deformation and the relative stiffness between pipes and soil. In order to investigate the effect of different soil properties on the deformation of the pipe, each layer was defined with specific parameters including thickness, unit weight, effective cohesion, angle of internal friction and modulus of elasticity (detailed in Table 1). The tunnel diameter, depth and pipe geometry parameters were kept constant throughout the analysis. Fig. 12 illustrated the settlement and stress of the pipeline in different soil layers, and the specific soil parameters are shown in Table 1. The stress in the lower part of the pipeline was generally the same in different strata, with the maximum value of 13.0 MPa occurring over the left tunnel axis. The settlement trough width and the maximum settlement of the pipeline in the silty sand strata were the largest, with a maximum settlement of 5.6 mm. Whereas the pipeline settlement was roughly the same in the other three strata, the maximum settlement was 4.3 mm. As shown in Table 1, there is no big difference between the soil parameters of the silty sand strata and other strata, except for the cohesive force which

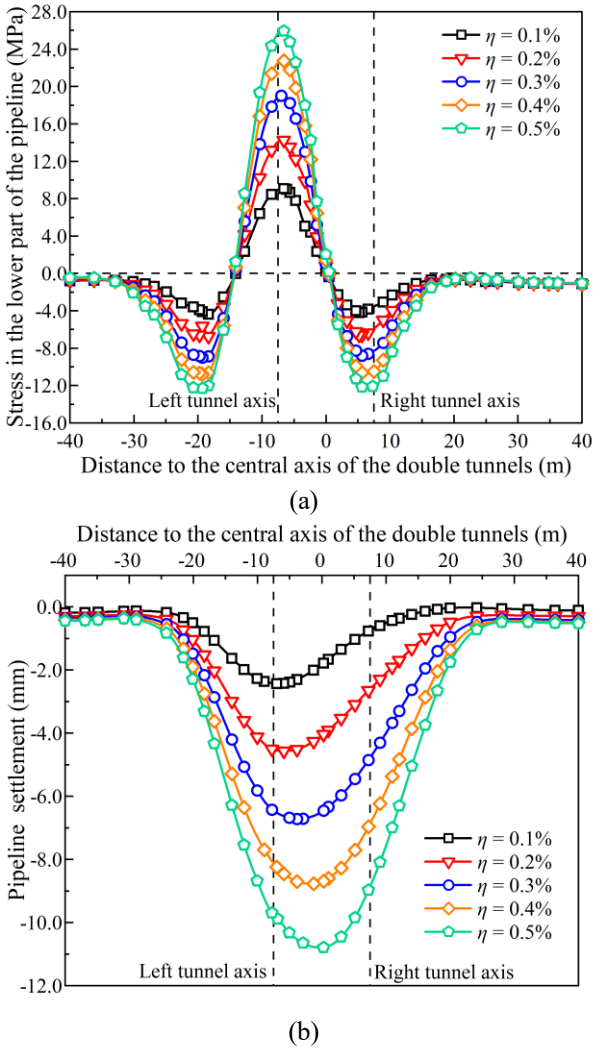

Fig. 11 Settlement and stress of pipes under different soil loss rates: (a) Stress after the left tunnel construction, (b) Pipeline settlement after double tunnel construction

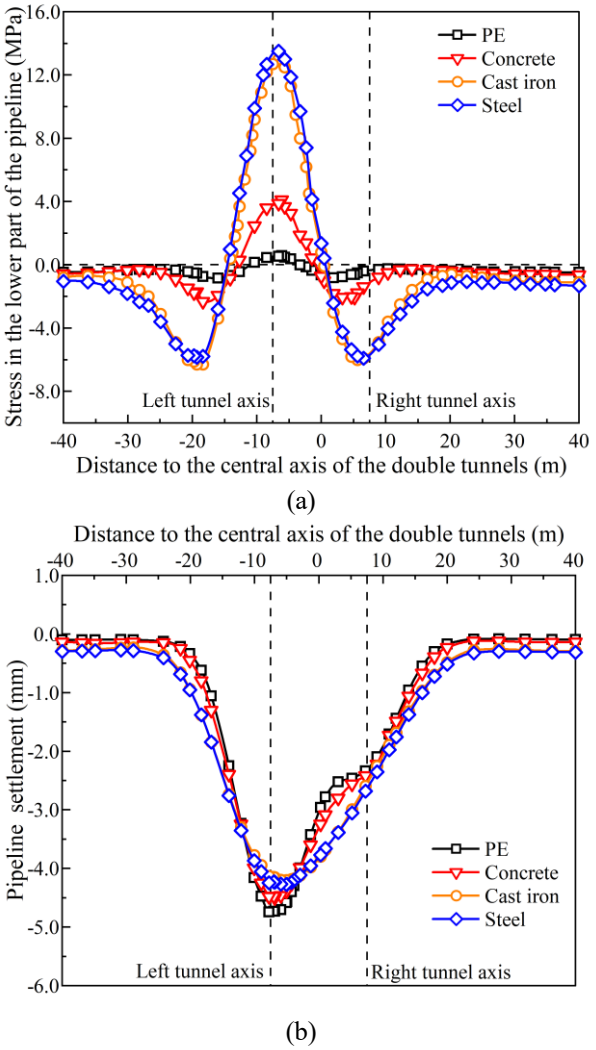

Fig. 12 Settlement and stress of pipelines with different materials: (a) Stress after the left tunnel construction and (b) Pipeline settlement after double tunnel construction

is much smaller than other strata. Therefore, the cohesive force of the soil strata where the pipeline was located played a dominant role in the pipeline settlement.

4.4.2 Soil loss rate

The soil loss caused by the void at the shield tail was the main reason for the pipeline settlement, as indicated by the analysis of the measured data in Section 3. Therefore, five different soil loss rates (η) were chosen for numerical simulation to analyze their effects on pipeline deformation. The settlement and stresses of the pipeline with different soil loss rates were shown in Fig. 13.

The stress in the lower part of the pipeline increased remarkably as the soil loss rate increased from 0.1% to 0.5%, the maximum tensile stress increased from 9 MPa to 28 MPa by 211%, and the maximum compressive stress increased from 5.0 MPa to 12.0 MPa by 140%. However, the location of the maximum stress occurred always remained the same. The pipeline settlement increased significantly with the increasing soil loss rate, and the position of the largest settlement moved from the upper of left tunnel axis to the upper of the double tunnel central axis. As the loss rate of soil increased from 0.1% to 0.5%, the maximum value of pipeline settlement increased from 2.5 mm to 11 mm, an increase of 340%.

In general, the soil loss rate had a huge impact on both the settlement and stress of the pipeline, which was consistent with the finding of Wei *et al*. (2016). And the increase in soil loss rate will cause a higher increase in settlement and stress of the pipeline. Choosing reasonable construction parameters and grouting at the shield tail in time to reduce soil loss is the key to guaranteeing the safety and normal use of the pipeline.

4.4.3 Pipeline material

The materials of the urban municipal pipelines vary considerably. Hence, four typical materials of the pipeline were chosen to simulate numerically, and the material characteristics were shown in Table 3. Fig. 14 illustrated the settlements and stresses of pipes in different materials. The settlements of cast iron and steel pipe were comparatively smaller, and the settlement curve presented V-shape,

whereas the settlements of PE and concrete pipe were larger, and the settlement curve was approximately featured W-shaped. Cast iron and steel pipes had relatively little settlement and exhibited V-shaped settling curves, whereas PE and concrete pipes had larger settlements and approximately exhibited W-shaped settling curves. It was mainly attributed to the less stiffness of PE pipe and concrete pipe, weaker ability to resist deformation, and better coordination with the deformation of the soil in their location. This is different from the conclusion drawn by Liu *et al.* (2011), which found no effect of different materials on pipeline settlement in clay strata.

Moreover, the greatest tensile stress of the pipeline increased with pipe stiffness, which was opposite to its effect on settlement. The maximum stress for PE pipe and steel pipe was 1.0 MPa and 14.2 Mpa respectively, which was the biggest difference. Consequently, cast iron pipes, steel pipes, and other highly rigid pipes are vulnerable to tensile damage in the actual construction owing to the relatively high tensile stresses they suffer. As for PE pipes, concrete pipes, and other less rigid pipes, leakage or rupture may occur owing to large deformations at the interface or corners of the pipeline.

4.4.4 Pipeline buried depth

The stresses and settlements of pipelines with different buried depths were shown in Fig. 15. As the pipeline buried depth increased, the maximum pipeline settlement increased firstly and decreased later, reaching the maximum value at 6m. This was mainly attributed to that the sedimentation in the layer where the pipe was located increased with depth, resulting in the increase of pipeline settlement. Whereas, as the pipeline gradually approached the top of the tunnel, the pipeline settlement was gradually decreased by the effect of grouting pressure. The stress in the lower part of the pipeline gradually increased with the buried depth increased from 2m to 8m, and the maximum tensile stress increased by 81.5% from 13.6 MPa to 24.5 MPa. Therefore, the increasing pipe burial depth had a greater impact on its stress and a relatively small impact on settlement.

5. Risk assessment of pipelines

There is no unified standard for risk assessment of pipeline deformation caused by shield tunnel construction. Since it is easiest to monitor the pipeline settlement, most of the specifications take 10 mm as the settlement limit value of large-diameter rigid pressurized pipes, and 80% and 65% of the accumulated settlement as the early warning value. The limit value and warning values of the settlement were adopted to classify pipeline safety risk levels, and the corresponding countermeasures were listed for different risk levels, as shown in Table 4, where S_{pmax} represents the maximum settlement of the pipeline.

Fig. 16 represented the layout of pipeline risk levels at the soil loss rate of 0.5%, which is the maximum value in actual construction. H_P and H_T denote the pipeline buried depth and tunnel buried depth, respectively, and L denotes the distance between two tunnels. It can be seen that the borderline of the

Table 4 Risk classification of large diameter rigid pressurized pipes in silty fine sand strata

Risk Level	Risk Description	Judgment Method	Recommended protection and response measures
I	High risk	$S_{pmax}>$ 10 mm	Relocating pipelines or breakage repair, and strengthening monitoring
II	Medium risk	8 mm $<S_{pmax}<$ 10 mm	Grouting reinforcement or suspending the pipeline, and strengthening monitoring
III	Low risk	6.5 mm $<S_{pmax}<$ 8 mm	Monitoring during the whole construction, and reinforcement measures can be adopted if necessary
IV	Minimum risk	$S_{pmax}<$ 6.5 mm	Monitoring the settlement during shield tunnel crossing pipelines

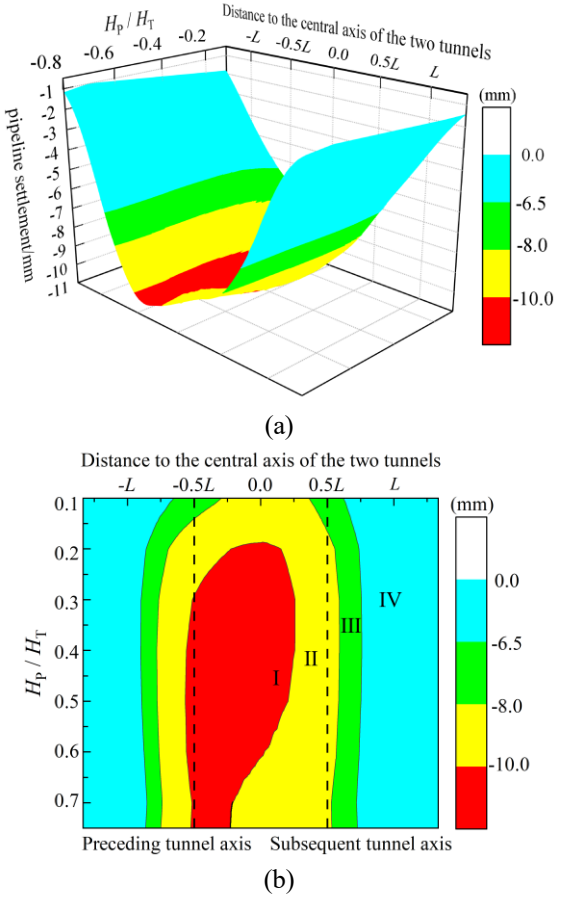

Fig. 13 Distribution of the risk level for pipelines: (a) 3D risk level distribution and (b) 2D projection

risk level extends towards the ground in an arc shape, and the high-risk area is mainly concentrated between the two tunnel axes and biased to the preceding tunnel axis. There is no high-risk area on the pipeline as H_P/H_T less than 0.2, and the high-risk area is the largest with the H_P/H_T of 0.3 to 0.5. As H_P/H_T increases from 0.5 to 0.7, the high-risk area of the pipeline gradually decreases owing to the effect of grouting under segments. And the high-risk area is only distributed within

0.25L of the inner side of the preceding tunnel axis as the H_P/H_T greater than 0.7. Moreover, the part of pipelines outside the 0.85L of the preceding tunnel axis and the 0.75L of the subsequent tunnel axis is in the minimum risk area. In summary, the risk status of the pipeline can be quickly identified by the risk level distribution map of the large diameter rigid pressurized pipes in silty fine sand strata, and thus corresponding protection measures can be taken.

6. Conclusions

In this paper, the impact of double shield tunneling on large-diameter pipelines in silty fine sand strata was investigated by field measurement and numerical simulations. The major findings are as below.

1. Compared with the perfectly symmetrical settling curve of the pipeline at the end of double tunnel construction in clay strata, the settling curve was not symmetrical in the silty fine sand strata, the position of the maximum settlement was biased towards the preceding tunnel.

2. The construction of the subsequent tunnel had significantly less impact on the stress and horizontal displacement of the pipeline than the preceding tunnel, but the impact on the settlement of the pipeline was almost the same.

3. There is a significant shading effect of the large-diameter pipeline, which would restrict the settlement of the soil above the pipeline in the tunnel construction.

4. The adjusted settlement formula shows good agreement with the measured data, facilitating approximate calculations for both surface and pipe settlements. The correction factor a ranges from 0.50 to 0.90, while b ranges from 0.95 to 1.20.

5. The elastic modulus and burial depth of the pipeline had a great effect on the stress of the pipeline, and a smaller effect on the settlement of the pipeline. However, the soil loss rate greatly affected both the settlement and stress of the pipeline, which would increase remarkably with the increasing soil loss rate.

6. The high-risk area of the large-diameter rigid pressurized pipes is mainly located between the two tunnel axes and biased to the preceding tunnel axis. The pipeline risk level distribution map can quickly identify the risk status of the pipeline and facilitate the timely adoption of protective measures.

By highlighting the asymmetrical settlement patterns and the differential impacts of tunnel sequences, it can inform engineering practices to mitigate risks. The shading effect of large-diameter pipes and the derived settlement formulas provide practical tools for predicting and managing soil behavior. Additionally, identifying high-risk areas enables proactive measures to safeguard pipeline integrity, ultimately improving infrastructure reliability in similar geological contexts.

While our findings enhance the understanding of tunneling and pipeline settling behavior, they are limited to silty fine sand strata, indicating a need for further research in other soil types. Future studies should focus on long-term pipeline monitoring in diverse soils, developing predictive models for various materials and configurations, and investigating mitigation strategies for the shading effect of large-diameter pipelines.

Acknowledgments

The research described in this paper was partially supported by the National Natural Science Foundation of China (Grant No. 51978159) and the National Key R&D Program of China (Grant No. 2015CB057803).

References

Asakura, T. and Kojima, Y. (2003), "Tunnel maintenance in Japan", *Tunn. Undergr. Sp. Tech.*, **18**(2), 161-169. https://doi.org/10.1016/S0886-7798(03)00024-5.

Boulefrakh, L., Hebali, H., Chikh, A., Bousahla, A.A., Tounsi, A. and Mahmoud, S.R. (2019), "The effect of parameters of visco-Pasternak foundation on the bending and vibration properties of a thick FG plate", *Geomech. Eng.*, **18**(2), 161-178. https://doi.org/10.12989/gae.2019.18.2.161.

Civalek, O. and Ozturk, B. (2010), "Free vibration analysis of tapered beam-column with pinned ends embedded in Winkler-Pasternak elastic foundation", *Geomech. Eng.*, **2**(1), 45-56. https://doi.org/10.12989/gae.2010.2.1.045.

Chen, R.P., Zhu, J., Liu, W. and Tang, X.W. (2011), "Ground movement induced by parallel EPB tunnels in silty soils", *Tunn. Undergr. Sp. Tech.*, **26**(1), 163-171. https://doi.org/10.1016/j.tust.2010.09.004.

Deng, H., Fu, H., Shi, Y., Huang, Z. and Huang, Q. (2021), "Analysis of asymmetrical deformation of surface and oblique pipeline caused by shield tunneling along curved section", *Symmetry*, **13**(12), 2396. https://doi.org/10.3390/sym13122396.

Ding, J., Zhang, S., Zhang, H., Guo, C., Liao, Z. and Liu, H. (2021), "Ground settlement caused by shield tunneling in soil-rock composite strata", *J. Perform. Constr. Fac.*, **35**(5), 04021057. https://doi.org/10.1061/(ASCE)CF.1943-5509.0001631.

Guan, X.M., Wang, G., Wang, X.C., An, J.Y., Lei, H.B. and Guan, W.Z. (2020), "Influences of shield tunnel construction of double-line metro on settlement of existing pipeline", *J. Eng. Sci. Tech. Rev.*, **13**(2), 167-173. https://doi.org/10.25103/jestr.132.20.

Hasanpour, R. (2014), "Advance numerical simulation of tunneling by using a double shield TBM", *Comput. Geotech.*, **57**, 37-52. https://doi.org/10.1016/j.compgeo.2014.01.002.

Heama, N., Jongpradist, P., Lueprasert, P., Suwansawat, S. and Jamsawang, P. (2021), "Comparative effects of adjacent loaded pile row on existing tunnel by 2D and 3D simulation models", *Geomech. Eng.*, **27**(2), 151-165. https://doi.org/10.12989/gae.2021.27.2.151.

Hu, X., Cheng, J. and Ju, J.W. (2021), "Influence of the cutterhead configuration and operation parameters on the face stability of EPB shield tunnels in dry granular soils", *Int. J. Geomech.*, **21**(5), 04021050. https://doi.org/10.1061/(ASCE)GM.1943-5622.0002008

Huang, M., Zhou, X., Yu, J., Leung, C.F. and Tan, J.Q.W. (2019), "Estimating the effects of tunnelling on existing jointed pipelines based on Winkler model", *Tunn. Undergr. Sp. Tech.*, **86**, 89-99. https://doi.org/10.1016/j.tust.2019.01.015

Jallow, A., Ou, C.Y. and Lim, A. (2019), "Three-dimensional numerical study of long-term settlement induced in shield tunneling", *Tunn. Undergr. Sp. Tech.*, **88**, 221-236. https://doi.org/10.1016/j.tust.2019.02.021.

Jeon, Y.J., Jeon, S.C., Jeon, S.J. and Lee, C.J. (2020), "Study on the behaviour of pre-existing single piles to adjacent shield tunnelling by considering the changes in the tunnel face pressures and the locations of the pile tips", *Geomech. Eng.*, **21**(2), 187-200. https://doi.org/10.12989/gae.2020.21.2.187.

Joshi, T., Parkash, O. and Krishan, G. (2023a), "Estimation of energy consumption and transportation characteristics for slurry flow through a horizontal straight pipe using computational fluid dynamics", *Phys. Fluids*, **35**(5). https://doi.org/10.1063/5.0146534.

Joshi, T., Parkash, O. and Krishan, G. (2023b), "Slurry flow characteristics through a horizontal pipeline at different Prandtl numbers", *Powder Technol.*, **413**, 118008. https://doi.org/10.1016/j.powtec.2022.118008.

Joshi, T., Parkash, O., Gallegos, R.K.B. and Krishan, G. (2024), "Parametric investigation of slurry transport: Computational insight into the impact of particle composition and Prandtl numbers", *Phys. Fluids*, **36**(2). https://doi.org/10.1063/5.0187126.

Jiao, N., Wan, X., Ding, J., Zhang, S. and Liu, J. (2024), "Pipeline deformation caused by double curved shield tunnel in soil-rock composite stratum", *Geomechanics and Engineering*, **36**(2), 131-143. https://doi.org/10.12989/gae.2024.36.2.131

Katebi, H., Rezaei, A. H., Hajialilue-Bonab, M., Tarifard, A. (2015), "Assessment the influence of ground stratification, tunnel and surface buildings specifications on shield tunnel lining loads (by FEM)", *Tunn. Undergr. Sp. Tech.*, **49**, 67-78. https://doi.org/10.1016/j.tust.2015.04.004.

Klar, A., Elkayam, I. and Marshall, A.M. (2016), "Design oriented linear-equivalent approach for evaluating the effect of tunneling on pipelines", *J. Geotech. Geoenviron. Eng.*, **142**(1), 04015062. https://doi.org/10.1061/(ASCE)GT.1943-5606.0001376.

Klar, A., Marshall, A.M., Soga, K. and Mair, R.J. (2008), "Tunneling effects on jointed pipelines", *Can. Geotech. J.*, **45**(1), 131-139. https://doi.org/10.1139/T07-068.

Klar, A., Vorster, T.E.B., Soga, K. and Mair, R.J. (2007), "Elastoplastic solution for soil-pipe-tunnel interaction", *J. Geotech. Geoenviron. Eng.*, **133**(7), 782-792. https://doi.org/10.1061/(ASCE)1090-0241(2007)133:7(782).

Li, L., Du, X. and Zhou, J. (2020), "Numerical simulation of site deformation induced by shield tunneling in typical upper-soft-lower-hard soil-rock composite stratum site of changchun", *KSCE J. Civil Eng.*, **24**(10), 3156-3168. https://doi.org/10.1007/s12205-020-0124-0.

Li, X., Wang, T. and Yang, Y. (2020), "An investigation into the tunnel-soil-pipeline interaction by in situ measured settlements of the pipelines", *Adv. Civil Eng.*, **2020**. https://doi.org/10.1155/2020/8850380.

Liu, G.S., Sun, L.W., Wang, B., Wu, S.M., Hong, C.P. and Hong, Q. (2012), "The numerical analysis and field measurements of the shield tunnel passing through the pipeline groups", *Appl. Mech. Mater.*, **226**, 1488-1494. https://doi.org/10.4028/www.scientific.net/amm.226-228.1488.

Liu, J.L. and Liu, J.Q. (2011), "Influence of tunnel excavation on adjacent underground pipeline", *Adv. Mater. Res.*, **150**, 1777-1781. https://doi.org/10.4028/www.scientific.net/amr.150-151.1777

Liu, X., Wang, F., Huang, J., Wang, S., Zhang, Z. and Nawnit, K. (2019), "Grout diffusion in silty fine sand stratum with high groundwater level for tunnel construction", *Tunn. Undergr. Sp. Tech.*, **93**, 103051. https://doi.org/10.1016/j.tust.2019.103051.

Mackett, R.L. and Edwards, M. (1998), "The impact of new urban public transport systems: will the expectations be met?", *Transportation Research Part A: Policy and practice*, **32**(4), 231-245. https://doi.org/10.1016/S0965-8564(97)00041-4.

Marshall, A.M., Klar, A. and Mair, R.J. (2010), "Tunneling beneath buried pipes: view of soil strain and its effect on pipeline behavior", *J. Geotech. Geoenviron. Eng.*, **136**(12), 1664-1672. https://doi.org/10.1061/(asce)gt.1943-5606.0000390.

Mathew, G.V. and Lehane, B.M. (2013), "Numerical back-analyses of greenfield settlement during tunnel boring", *Can. Geotech. J.*, **50**(2), 145-152. https://doi.org/10.1139/cgj-2011-0358

Möller, S.C. and Vermeer, P.A. (2008), "On numerical simulation of tunnel installation", *Tunn. Undergr. Sp. Tech.*, **23**(4), 461-475. https://doi.org/10.1016/j.tust.2007.08.004.

Nawel, B. and Salah, M. (2015), "Numerical modeling of two parallel tunnels interaction using three-dimensional finite elements method", *Geomech. Eng.*, **9**(6), 775-791. https://doi.org/10.12989/gae.2015.9.6.775.

Ocak, I. (2013), "Interaction of longitudinal surface settlements for twin tunnels in shallow and soft soils: the case of Istanbul Metro", *Environ. Earth Sci.*, **69**(5), 1673-1683. https://doi.org/10.1007/s12665-012-2002-7.

Peck, R.B. (1969), "Deep excavations and tunneling in soft ground", *Proceedings of the 7th International Conference on Mechanics and Foundation Engineering*, Mexico City, Mexico.

Rezaei, A.H., Shirzehhagh, M. and Golpasand, M.R.B. (2019), "EPB tunneling in cohesionless soils: A study on Tabriz Metro settlements", *Geomech. Eng.*, **19**(2), 153-165. https://doi.org/10.12989/gae.2019.19.2.153.

Rowe, R.K., Lo, K.Y. and Kack, G.J. (1983), "A method of estimating surface settlement above tunnels constructed in soft ground", *Can. Geotech. J.*, **20**(1), 11-22. https://doi.org/10.1139/t83-002.

Sae-Long, W., Limkatanyu, S., Hansapinyo, C., Prachasaree, W., Rungamornrat, J. and Kwon, M. (2021), "Nonlinear flexibility-based beam element on Winkler-Pasternak foundation", *Geomech. Eng.*, **24**(4), 371-388. https://doi.org/10.12989/gae.2021.24.4.371.

Sarfarazi, V. and Tabaroei, A. (2020), "Numerical simulation of the influence of interaction between Qanat and tunnel on the ground settlement", *Geomech Eng.*, **23**(5), 455-466. https://doi.org/10.12989/gae.2020.23.5.455.

Shi, P. (2015), "Surface wave propagation effects on buried segmented pipelines", *J. Rock Mech. Geotech. Eng.*, **7**(4), 440-451, https://doi.org/ 10.1016/j.jrmge.2015.02.011

Sun, S., Rong, C., Wang, H., Cui, L. and Shi, X. (2021), "The ground settlement and the existing pipeline response induced by the nonsynchronous construction of a twin-tunnel", *Adv. Civil Eng.*, **2021**. https://doi.org/10.1155/2021/8815304.

Suwansawat, S. and Einstein, H.H. (2007), "Describing settlement troughs over twin tunnels using a superposition technique", *J. Geotech Geoenviron. Eng.*, **133**(4), 445-468. https://doi.org/10.1061/(ASCE)1090-0241(2007)133:4(445).

Vorster, T.E., Klar, A., Soga, K. and Mair, R.J. (2005), "Estimating the effects of tunneling on existing pipelines", *J. Geotech. Geoenviron. Eng.*, **131**(11), 1399-1410. https://doi.org/10.1061/(ASCE)1090-0241(2005)131:11(1399).

Wang, J., Cao, A., Wu, Z., Wang, H., Liu, X., Li, H. and Sun, Y. (2021), "Experiment and numerical simulation on grouting reinforcement parameters of ultra-shallow buried double-arch tunnel", *Appl. Sci.*, **11**(21), 10491. https://doi.org/10.3390/app112110491.

Wei, G., Hu, S., Xing, J.J. and Ye, Q. (2016), "Effect of double-line parallel shield excavation on adjacent underground pipelines", *J. Eng. Sci. Tech. Rev.*, **9**(1), 167-173. https://doi.org/10.25103/jestr.091.25.

Wham, B.P., Argyrou, C. and O'Rourke, T.D. (2016), "Jointed pipeline response to tunneling-induced ground deformation", *Can. Geotech. J.*, **53**(11), 1794-1806. https://doi.org/10.1139/cgj-2016-0054.

Zhang, C., Yu, J. and Huang, M. (2012), "Effects of tunnelling on existing pipelines in layered soils", *Comput. Geotech.*, **43**, 12-25. https://doi.org/10.1016/j.compgeo.2012.01.011.

Zhang, Z., Xu, W., Nie, W. and Deng, L. (2021), "DEM and theoretical analyses of the face stability of shallow shield cross-river tunnels in silty fine sand", *Comput. Geotech.*, **130**,

103905. https://doi.org/10.1016/j.compgeo.2020.103905.
Zhu, J. and Zhu, D. (2020), "Deformation of pipelines induced by the construction of underlying twin-tunnel", *Tehnicki Vjesnik - Technical Gazette*, **27**(4), 1311-1315. https://doi.org/10.17559/tv-20191118080659.

JS